Signatures of Impurities in 1- and 2-dimensional Lattice and Continuum Models for Metals

Author:
T.X. van der Meijden

Supervisor:
Dr. L. Fritz

September 2017 - January 2018

Universiteit Utrecht

Abstract

This thesis develops a method of quantitatively describing the effects of inserting an impurity into a one- or two-dimensional crystal. Firstly, the Green's function, a mathematical function necessary to find the density of states for such a system, is introduced. From there on, the thesis will proceed to finding the eigenenergies for the pure crystals using an exact and an approximate method. The impurity is then inserted in the form of a Dirac delta potential and the results of both methods are compared. For low energies the two methods reinforce each other and the results indicate that particles wish to scatter of with specific momenta and some positions are unfavorable to be occupied. For higher energies the approximation is no longer viable and results differ from the exact results.

Acknowledgements

I would first like to thank the entire research group for Condensed Matter Theory. In particular and foremost I want to thank dr. Lars Fritz who inspired me to dive deeper into this field of research and who took the time for our weekly meetings. Secondly, I would like to thank Gerwin for maintaining a seemingly open door policy for any questions that puzzled me and allowing me to read up on the relevant chapters of his Master's thesis. Lastly, I would like to express my gratitude to my friends for the discussions and studying sessions and most of all Yoran Tournois for the useful tips and comments on the writing of this thesis.

Contents

1 Introduction

In solid-state physics the characteristics of a solid are governed by the underlying geometry of the structure between its molecules or atoms. The conductivity, rigidity or specific heat of a crystal can all be contributed to this crystal structure. Recently, this field has become more interesting. In 2010 the Nobel Prize in Physics was awarded to André Geim and Konstantin Novoselov for characterizing graphene, a hexagonal carboncrystal with desirable conductivity, both electronic and thermal [1]. Graphene's high conductivity is due to the fact that the electrons inside can move easily from atom to atom as they have effectively lost their mass.

The behavior of materials is often greatly impacted by their purity or impurity. Nature rarely produces pure crystals and often leaves small imperfections. These impurities or defects range from a vacancy at one site to an entirely different atom being situated at said site. Having a different atom at the site can make this a more or less favorable site for electrons to occupy. Alloys (intermetallic compounds) are an example where substituting atoms can result in much more useful materials [2]. There is also the concept of doping where silicon may be altered by inserting an atom with an electron more (or less) in the valence shell to tune the material's properties. These alterations are reflected in the *density of states*. This thesis will give insight in the effect of single impurities by comparing the crystals to their pure counterparts.

In Section 2 we will introduce the Green's function. This function is an essential and powerful tool to get reliable results for the density of states. In Section 3 the lattice model is discussed and approximated as a continuum. We will then proceed by finding the density of states for the pure crystals. Sections 4 and 5 are aimed towards finding the density of states for the crystals with an impurity inserted and comparing the approximate and exact results. Lastly, Section 6 concludes by evaluating the results found in this thesis.

2 The Green's Function

In this section we will give an introduction to the Green's function, an essential asset in finding certain characteristics of systems such as the density of states. To start we will give a formal introduction and then use its definition to find an expression for the density of states. From this point on we will closely follow [4] to find an expression for the Green's function and relate it to the density of states.

2.1 Introducing the Green's Function

Originally introduced to help solve linear differential equations, the Green's function is any solution of the equation

$$LG\left(x,s\right)=\delta\left(x-s\right), \tag{1}$$

where L is a linear differential operator and $\delta\left(x-s\right)$ is the Dirac delta function[1] [5]. If we now look at the eigenfunctions $\psi_n\left(x\right)$ for which

$$L\psi_n\left(x\right)=\lambda_n\psi_n\left(x\right) \tag{2}$$

holds, we can perhaps already see that the Green's function can be used for the Schrödinger equation;

$$\left(E-H\right)G\left(x,x',E\right)=\delta\left(x-x'\right). \tag{3}$$

Using the equation above together with following relations in bra ket notation:

$$\begin{aligned}\delta\left(x-x'\right)&=\langle x|x'\rangle \\ \mathbb{I}&=\int dx|x\rangle\langle x| \\ H\left(x\right)\delta\left(x-x'\right)&=E\langle x|x'\rangle \\ &\equiv\langle x|H|x'\rangle \\ G\left(x,x',E\right)&\equiv\langle x|G\left(E\right)|x'\rangle,\end{aligned} \tag{4}$$

one can rewrite Eq. (3) to

$$\left(E-H\right)G\left(E\right)=\mathbb{I}, \tag{5}$$

and then use the identities from Eqs. (4) to find the matrix element of Eq. (5) corresponding to the elements (x,x'):

[1] Here we are assuming a continuous system. A square lattice would be discrete and we would substitute $G\left(x,s\right)$ by G_{xs} and $\delta\left(x-s\right)$ by δ_{xs}.

$$\begin{aligned}\langle x|\left(E-H\right)G\left(E\right)|x'\rangle &= \langle x|EG\left(E\right)|x'\rangle - \langle x|HG\left(E\right)|x'\rangle \\ &= EG\left(x,x',E\right) - \langle x|HG\left(E\right)|x'\rangle \\ &= EG\left(x,x',E\right) - H\left(x\right)\langle x|G\left(E\right)|x'\rangle \\ &= EG\left(x,x',E\right) - H\left(x\right)G\left(x,x',E\right), \end{aligned} \tag{6}$$

and taking the same matrix element on the righthandside we end up with:

$$EG\left(x,x',E\right) - H\left(x\right)G\left(x,x',E\right) = \delta\left(x-x'\right). \tag{7}$$

When none of the eigenvalues of $E-H$ are equal to 0, we can find from Eq. (5)

$$G\left(E\right) = \left(E-H\right)^{-1}. \tag{8}$$

Multiplying this expression with an identity matrix, we find:

$$G\left(E\right) = \sum_n \frac{\psi_n\left(x\right)\psi_n^\star\left(x'\right)}{E-E_n}. \tag{9}$$

A mindful reader will notice that when the energy is at an eigenenergy level, the Green's function diverges. To make sure the Green's function is still defined at these essential points we add an infinitesimal, imaginary value η to the energy. This version of the Green's function we will denote as the *retarded Green's function:*

$$G^R\left(E\right) = \lim_{\eta\to 0^+}\sum_n \frac{\psi_n\left(x\right)\psi^\star\left(x'\right)}{E+i\eta-E_n}. \tag{10}$$

2.2 The Green's Function for Impurities

To complete our arsenal of Green's functions we still need to make one important distinction. Suppose we have a Hamiltonian H which we decompose as $H = H_0 + H_I$ where H_0 is the bare Hamiltonian (the kinetic part) and H_I is the interacting part (the potential). In Sections 4 and 5 we will consider a Hamiltonian describing a single impurity, i.e. with a constant potential except for one site[2]. Now we can make the distinction between the *bare Green's function* and the *total Green's function.* The bare Green's function,

$$G_0^R\left(E\right) = \lim_{\eta\to 0^+}\left(E+i\eta-H_0\right)^{-1}, \tag{11}$$

[2]We will discuss a scattering potential in detail in Sections 4 and 5 and briefly discuss an attractive potential in Section 4.1.4.

is solely dependent on the bare Hamiltonian, while the total Green's function depends on the full Hamiltonian.

The total Green's function can be calculated by inserting the full Hamiltonian;

$$\begin{aligned} G^R(E) &= \lim_{\eta\to 0^+} (E + i\eta - H_0 - H_I)^{-1} \\ &= \lim_{\eta\to 0^+} \Big((E + i\eta - H_0) \Big(\mathbb{I} - (E + i\eta - H_0)^{-1} H_I \Big) \Big)^{-1} \\ &= \left(\mathbb{I} - G_0^R(E) H_I \right)^{-1} G_0^R(E) \\ &= G_0^R(E) + G_0^R(E) H_I G_0^R(E) + G_0^R(E) H_I G_0^R(E) H_I G_0^R(E) + \ldots, \end{aligned} \tag{12}$$

where we have used the series expansion of $(\mathbb{I} - A)^{-1} = \mathbb{I} + A + A^2 + \ldots$ for square matrices A to reach the final line. To make this cumbersome expression easier to read, we will introduce the *T-matrix,* defined as[3]:

$$\begin{aligned} T(E) &\equiv H_I + G_0^R(E) H_I G_0^R(E) + \ldots \\ &= (\mathbb{I} - G_0^R(E) H_I)^{-1} H_I. \end{aligned} \tag{13}$$

With this matrix the expression for the operator $G^R(E)$ becomes

$$G^R(E) = G_0^R(E) + G_0^R(E) T(E) G_0^R(E). \tag{14}$$

Now that we have an expression for the Green's function as an operator finding an expression for the Green function is a possibility. The Green function is useful as it will pave the way towards finding the *local density of states* $\rho(\vec{r}, E)$ (LDOS) which we will discuss in Sections 4.1 and 5.1. As expressed in Eq. (4) the Green's function can be found using:

$$G^R(x, x', E) = \langle x | G^R(E) | x' \rangle. \tag{15}$$

If we now insert the expression found in (14) into this equation we find that

$$G^R(x, x', E) = G_0^R(x - x', E) + G_0^R(x, E) T(E) G_0^R(-x', E), \tag{16}$$

where we have inserted an impurity at $x = 0$ which alters the second term. There are a few things worth noting. The first term is now dependent on $x - x'$ as it is solely dependent on the bare Hamiltonian and is therefore translationally invariant (i.e. $G(x + x_0, x' + x_0, E) = G(x, x'E)$). This term describes moving from point x towards x' with no interaction with the potential.

[3] Usually this matrix is very sparse and in our case we will only have one non-zero element. It can be interpreted as accounting for scattering onto the impurity any amount of times as Eq. (12) indicates.

The second term makes up for all other propagations where a particle may scatter once, twice or any times off of the impurity at $x = 0$. This can be written with a bare Green's function hopping to the impurity. Then the T-matrix accounts for all possible scatterings and another bare Green's function to then hop from the impurity to x'.

2.3 The Green's Function and the Density of States

To see the relation between the Green's function and the density of states we start at the most basic expression of the density of states $\rho(E)$,

$$\rho(E) = \sum_n \delta(E - E_n). \tag{17}$$

From this point we can find the LDOS by simply multiplying by the probability to find a particle at x:

$$\rho(x, E) = \sum_n \delta(E - E_n) |\langle x|\psi_n\rangle|^2. \tag{18}$$

To now see the relation between the density of states and the Green's function a different definition is needed for the Dirac delta function:

$$\delta(x) = \lim_{\eta \to 0^+} \frac{1}{\pi} \frac{\eta}{x^2 + \eta^2}. \tag{19}$$

To motivate this definition, note that for any x different than $x = 0$ this equals zero as $\eta \to 0$. When $x = 0$ the function reduces to $\lim_{\eta\to 0^+} \frac{1}{\pi}\frac{1}{\eta}$ and this tends to infinity. These two domains are what define the Dirac delta function. As a last condition we must check the normalization,

$$\begin{aligned}
\int_{-\infty}^{\infty} \delta(x) &= \lim_{\eta \to 0^+} \int_{-\infty}^{\infty} dx \frac{1}{\pi} \frac{\eta}{x^2 + \eta^2} \\
&= \lim_{\eta \to 0^+} \int_{-\infty}^{\infty} dx \frac{1}{\pi\eta} \frac{1}{\left(\frac{x}{\eta}\right)^2 + 1} \\
&= \lim_{\eta \to 0^+} \int_{-\infty}^{\infty} \frac{1}{\pi} \frac{dy}{y^2 + 1} \\
&= \int_{-\pi/2}^{\pi/2} \frac{du}{\cos^2(u)} \frac{1}{\pi} \frac{1}{\tan^2(u) + 1} \\
&= \int_{-\pi/2}^{\pi/2} \frac{du}{\pi} \frac{1}{\cos^2(u) + \sin^2(u)} \\
&= 1.
\end{aligned}$$

Here we have used the substitutions that $y = \frac{x}{\eta}$ and then $\tan(u) = y$. From this we can see that as $\eta \to 0$, $y \to \pm\infty$, which in turn implies $u \to \pm\frac{\pi}{2}$. This proves the behavior of our expression is the same as that of the Dirac delta function[4]. Now we can fill in Eq. (18) with this expression:

$$\begin{aligned}
\rho(x,E) &= \lim_{\eta\to 0^+} \sum_n \frac{1}{\pi} \frac{\eta}{(E-E_n)^2+\eta^2} |\langle\psi_n|x\rangle|^2 \\
&= -\frac{1}{\pi} \lim_{\eta\to 0^+} \sum_n \mathrm{Im} \frac{1}{E+i\eta-E_n} \langle x|\psi_n\rangle\langle\psi_n|x\rangle \\
&= -\frac{1}{\pi} \mathrm{Im} \lim_{\eta\to 0^+} \sum_n \langle x| \frac{1}{E+i\eta-E_n} |\psi_n\rangle\langle\psi_n|x\rangle
\end{aligned}$$

Now we can realize that in the final line we can replace E_n by H;

$$\begin{aligned}
&= -\frac{1}{\pi} \mathrm{Im} \lim_{\eta\to 0^+} \sum_n \langle x| \frac{1}{E+i\eta-H} |\psi_n\rangle\langle\psi_n|x\rangle \\
&= -\frac{1}{\pi} \mathrm{Im} \lim_{\eta\to 0^+} \sum_n \langle x| \left(E+i\eta-H\right)^{-1} |x\rangle \\
&= -\frac{1}{\pi} \mathrm{Im}\, G^R(x,x,E)\,. \qquad (20)
\end{aligned}$$

Note that we have used $\frac{1}{x+i\eta} = \frac{x-i\eta}{x^2+\eta^2}$ to arrive at the second line of the derivation. Furthermore it should be noted that we have only taken the retarded Green's function as a solution while there is also the option of an advanced Green's function which has a different sign and instead of a positive infinitesimal amount η it adds a negative amount η. Since we will not use the advanced Green's function, we disregard it.

[4]Consequently, this also means we can replace $\lim_{\eta\to 0^+}$ with the y-integral from $-\infty$ to ∞. In the next line we use that $\tan(u) \to \pm\infty$ as $u \to \pm\frac{\pi}{2}$ to get the final result.

3 Lattice Model and Continuum Approximation

This section will look at the two relevant systems that will be discussed for the rest of the thesis. First, it will introduce the one-dimensional monatomic chain, find its eigenenergies, approximate it using a quadratic dispersion to then find the density of states for both expressions for the eigenenergies and compare them. Afterwards this will be repeated for a two-dimensional square lattice.

3.1 A Monatomic Chain

Let us take the most basic crystal we can think of; a monatomic chain of equidistant sites. Let α be the lattice constant and N the amount of atoms (Fig. 1). For simplicity we will assume each atom only has one orbital and which may be occupied by a single electron due to the Pauli exclusion principle[5] [8]. It is

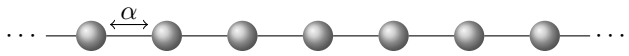

Figure 1: A monatomic chain of equidistant sites.

possible for electrons to leave one site and enter another site. This phenomenon is called *hopping*. Suppose this hopping is characterized by a hopping constant t, which is the probability amplitude for an electron to hop to a nearest neighbor site. Combined with a chemical potential μ the discrete Schrödinger equation will then be of a form

$$H_{ij} = -t\left(\delta_{i,j+1} + \delta_{i,j-1}\right) - \mu\delta_{i,j}, \tag{21}$$

where we note that with periodic boundary conditions we will use $N+1=1$. As the Hamiltonian is periodic it can be Fourier transformed to find the system's dependence on the momentum k. The Fourier transformation yields:

$$\begin{aligned} H_{kk'} &= -\frac{t}{N}\sum_{i,j}^{N}\left(e^{-iki\alpha}e^{-ik'j\alpha}\delta_{i,j+1} + e^{-iki\alpha}e^{-ik'j\alpha}\delta_{i,j-1}\right) - \frac{\mu}{N}\sum e^{-iki\alpha}e^{-ik'j\alpha}\delta_{i,j} \\ &= -\frac{t}{N}\sum_{i}^{N}\left(e^{-iki\alpha}e^{-ik'(i-1)\alpha} + e^{-iki\alpha}e^{-ik'(i+1)\alpha}\right) - \frac{\mu}{N}\sum_{i}^{N}e^{-iki\alpha}e^{-ik'i\alpha} \\ &= -\frac{t}{N}\sum_{i}^{N}\left(e^{-i\left(k+k'\right)i\alpha}e^{-ik'\alpha} + e^{i\left(k+k'\right)i\alpha}e^{ik'\alpha}\right) - \frac{\mu}{N}\sum_{i}^{N}e^{-i\left(k+k'\right)i\alpha}. \end{aligned}$$

After using the relation $\delta_{k,-k'} = \frac{1}{N}\sum_n e^{i\left(k+k'\right)n}$ it is clear to see that

[5] Strictly speaking states could be occupied by both a down-spin and up-spin electron, but for simplicity we ignore spin.

$$H_k = -\left(2t\cos\left(k\alpha\right) + \mu\right), \tag{22}$$

from which we can conclude that the eigenenergies are given by:

$$E_k = -2t\cos\left(k\alpha\right) - \mu. \tag{23}$$

3.1.1 Approximating the Eigenenergies

As presented in Eq. (23) the eigenenergies for the monatomic chain are given by $E_k = -2t\cos\left(k\alpha\right) - \mu$. Now we we will look at an approximation for low momenta. For this to be a realistic approximation we need to set μ such that we are in the lower part of the energy band as seen in Fig. 2, i.e. $\mu \approx -2$. In the particular case of a cosine function we can approximate:

$$\cos\left(k\alpha\right) \approx 1 - \alpha^2\frac{k^2}{2} + \ldots \tag{24}$$

and as a result can approximate the eigenenergies as:

$$E_k \approx t\alpha^2k^2 - \bar{\mu} \tag{25}$$

For the rest of the one dimensional case we will set $\bar{\mu} = 0$. In Fig. 2 it is clear the approximation works well for small k, but deviates for larger values, which we will keep in mind throughout[6].

Figure 2: The exact $(-2t\cos\left(k\alpha\right) - \mu)$ and approximate $(-t\alpha^2k^2)$ eigenenergies shown in red and orange respectively. Here $\mu = 2$.

[6]For all numerical results α and t have been set to 1.

3.1.2 The Density of States

To find the bare density of states $\rho_0(E)$ we can use the approximation found above and start by filling in Eq. (20) with a **bare** Green's function

$$\rho_0(E) = -\frac{1}{\pi}\mathrm{Im}\left(G_0^R(0,E)\right). \tag{26}$$

As we do not have an expression for the eigenenergies (and thus the Green's function) dependent on x we must use $G(k,E)$ and perform a Fourier transformation:

$$\begin{aligned} G_0^R(x,E) &= \lim_{\eta\to 0^+}\int_{-\infty}^{\infty}\frac{dk}{2\pi}\frac{e^{ikx}}{E+i\eta-t\alpha^2k^2} \\ &= \lim_{\eta\to 0^+}\int_{-\infty}^{\infty}\frac{dk}{2\pi}\frac{e^{ikx}}{\omega-t\alpha^2k^2}, \end{aligned} \tag{27}$$

where we have made the substitution $\omega = E + i\eta$.

We will not calculate this integral explicitly, but rather see it as a component of a contour integral consisting of a straight line along the real axis from $-a$ to a to then loop back with a semi-circle of radius a (Fig. 3). In Fig. 3 a possible pole has been indicated with j. For a contour integral we know it is proportional to the sum of residues residing inside the contour thanks to the Residue theorem [6];

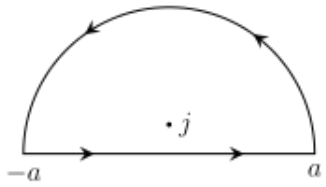

Figure 3: The contour for integration.

$$\begin{aligned} \lim_{a\to\infty}\int_{-a}^{a}dk\frac{e^{ikx}}{\omega-t\alpha^2k^2} + \int_{\mathrm{arc}}\lim_{a\to\infty}dk\frac{e^{i\vec{k}\cdot\vec{x}}}{\omega-t\alpha^2a^2} \\ = 2\pi i\cdot\mathrm{Res}\left(\frac{e^{ikx}}{\omega-t\alpha^2k^2}, k_{\mathrm{pole}}\right), \end{aligned} \tag{28}$$

where $\mathrm{Res}(f(k), k_{\mathrm{pole}})$ gives us the residue of the function at the pole located at k_{pole}. What is important is to realize is that the second integral will go to zero as a goes to infinity. This as k is a positive imaginary number and thus the exponent becomes $e^{-\mathrm{Im}(k)x}$ which goes to zero. To add upon this, the denominator also goes to infinity which nullifies the expression even quicker. This means the second term can be disregarded and we end up with

$$\lim_{a\to\infty}\int_{-a}^{a}dk\frac{e^{ikx}}{\omega-t\alpha^2k^2} = 2\pi i\cdot\mathrm{Res}\left(\frac{e^{ikx}}{\omega-t\alpha^2k^2}, k_{\mathrm{pole}}\right). \tag{29}$$

Some basic rewriting shows us that $k_{\text{pole}} = \pm\sqrt{\frac{\omega}{t\alpha^2}}$. Combining this with the definition of $\text{Res}(f(k), k_{\text{pole}}) \equiv \lim_{k\to k_{\text{pole}}}(k - k_{\text{pole}}) f(k)$ grants us for $x > 0$:

$$\begin{aligned}\lim_{a\to\infty}\int_{-a}^{a} dk \frac{e^{ikx}}{\omega - t\alpha^2 k^2} &= 2\pi i \cdot \lim_{k\to k_{\text{pole}}}(k - k_{\text{pole}})\left(\frac{e^{ikx}}{\omega - t\alpha^2 k^2}\right) \\ &= 2\pi i \cdot \lim_{k\to k_{\text{pole}}} \frac{e^{ikx}}{-2t\alpha^2 k} \\ &= -\pi i \cdot \sqrt{\frac{1}{t\alpha^2\omega}} \exp\left[i\sqrt{\frac{\omega}{t\alpha^2}}x\right]. \end{aligned} \tag{30}$$

What there is yet to see is that for $x < 0$ we can repeat the same process but now for a contour in the negative imaginary plane. This yields

$$\lim_{a\to\infty}\int_{-a}^{a} dk \frac{e^{ikx}}{\omega - t\alpha^2 k^2} = -\pi i \cdot \sqrt{\frac{1}{t\alpha^2\omega}} \exp\left[-i\sqrt{\frac{\omega}{t\alpha^2}}x\right] \tag{31}$$

and combining Eqs. (30) and (31) with Eq. (26):

$$G_0^R(x, E) = \lim_{\eta\to 0^+} -\frac{1}{2}\left[i\sqrt{\frac{1}{t\alpha^2\omega}} \exp\left(i\sqrt{\frac{\omega}{t\alpha^2}}|x|\right)\right]. \tag{32}$$

From this we can find the bare density of states (i.e. without an impurity):

$$\begin{aligned}\rho_0(E) &= \frac{1}{2\pi}\lim_{\eta\to 0^+} \text{Im}\left[i\sqrt{\frac{1}{t\alpha^2\omega}}\right] \\ &= \frac{1}{2\pi}\lim_{\eta\to 0^+} \text{Re}\left[\sqrt{\frac{1}{t\alpha^2\omega}}\right] \qquad (33) \\ &= \frac{1}{2\pi}\lim_{\eta\to 0^+} \sqrt{\frac{1}{t\alpha^2 E}}\Theta(E), \qquad (34)\end{aligned}$$

where $\Theta(E)$ is the Heaviside function defined to be 0 for $E < 0$ and 1 for $E \geq 0$.

3.1.3 Comparison of the Exact and Approximate Density of States

For this relatively simple case we can also calculate the exact density of states. To get an idea of how accurate our method is, we will calculate the bare density of states exactly and compare the results.

We will start out with the expression for the density of states using the Green's function:

$$\begin{aligned}
\rho_0(E) &= -\frac{1}{\pi}\mathrm{Im}\left[\int_{-\pi}^{\pi}\frac{dk}{2\pi}\frac{1}{E+i\eta+\mu+2t\cos(k\alpha)}\right] \\
&= -\frac{1}{\pi}\mathrm{Im}\left[\int_{-\pi}^{\pi}\frac{dk}{2\pi}\frac{1}{E+i\eta+\mu+t\left(e^{ik\alpha}+e^{-ik\alpha}\right)}\right] \\
&= -\frac{1}{\pi}\mathrm{Im}\left[\oint_C\frac{dz}{2\pi i\alpha z}\frac{1}{E+i\eta+\mu+t\left(z+z^{-1}\right)}\right] \\
&= -\frac{1}{\pi}\mathrm{Im}\left[\oint_C\frac{dz}{2\pi i\alpha}\frac{1}{tz^2+z\left(E+i\eta+\mu\right)+t}\right], \qquad (35)
\end{aligned}$$

where we have made the substitution $z = e^{ik\alpha}$ and C is the contour of a circle from -1 counterclockwise. For this integral we can once again use the Residue theorem

$$\begin{aligned}
\rho_0(E) &= -\frac{1}{\pi t\alpha}\mathrm{Im}\left[\mathrm{Res}\left(\frac{1}{z^2+z\frac{E+i\eta+\mu}{t}+1}\right), z_{\mathrm{pole}}\right] \\
&= -\frac{1}{\pi t\alpha}\mathrm{Im}\left[\lim_{z\to z_{\mathrm{pole}}}\frac{z-z_{\mathrm{pole}}}{z^2+z\frac{E+i\eta+\mu}{t}+1}\right] \\
&= -\frac{1}{\pi t\alpha}\mathrm{Im}\left[\lim_{z\to z_{\mathrm{pole}}}\frac{1}{2z+\frac{E+i\eta+\mu}{t}}\right]. \qquad (36)
\end{aligned}$$

Note that $z_{\mathrm{pole}} = \frac{1}{2}\left(-\frac{E+i\eta+\mu}{t} \pm \sqrt{\left(\frac{E+i\eta+\mu}{t}\right)^2-4}\right)$ but we are only interested in the pole in the positive imaginary plane which results in

$$\begin{aligned}\rho_0(E) &= \frac{1}{\pi t\alpha}\mathrm{Im}\left[\frac{1}{\sqrt{\left(\frac{E+\mu}{t}\right)^2-4}}\right] \\ &= \frac{1}{2\pi t\alpha}\mathrm{Im}\left[-i\frac{1}{\sqrt{1-\left(\frac{E+\mu}{2t}\right)^2}}\right] \\ &= \frac{1}{2\pi t\alpha}\frac{1}{\sqrt{1-\left(\frac{E+\mu}{2}\right)}}\Theta\left(4-(E+\mu)^2\right). \end{aligned} \tag{37}$$

As to be expected the approximation holds well for small μ so that the eigenenergies behave similarly and the discrepancy only shows up for the greater eigenenergies (Fig. 4).

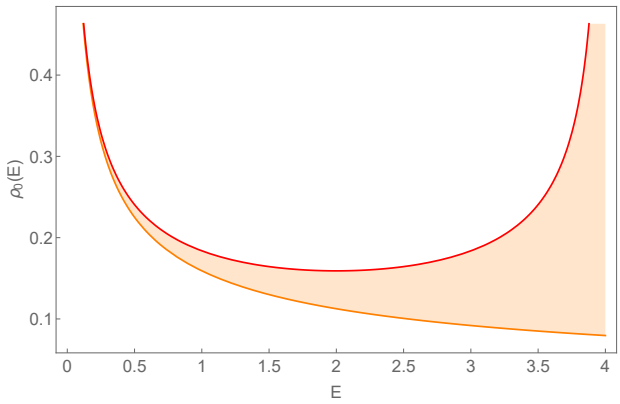

Figure 4: The exact and approximate bare density of states shown in red and orange respectively. For the exact solution we set $\mu = -2$ and furthermore we have set $\eta = 0.0001$.

3.2 A Square Lattice

For this case we simply make some alterations to the Hamiltonian found previously. Let us take a square $N \times N$ lattice in the x, y-plane with a lattice constant α (Fig. 5).

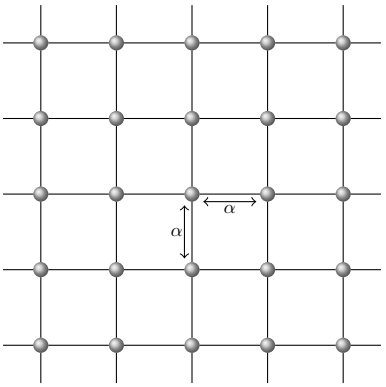

Figure 5: A square lattice of equidistant sites.

What we need to note is the amount of possible hops. At site (x, y) an electron can hop to four neighboring sites; $(x + \alpha, y)$, $(x, y + \alpha)$, $(x - \alpha, y)$ and $(x, y - \alpha)$. This gives four hopping terms in our Hamiltonian;

$$\begin{aligned} H_{x,x',y,y'} = &- t\left[\delta_{x,x'}\delta_{y,y'+1} + \delta_{x,x'}\delta_{y,y'-1} + \delta_{x,x'+1}\delta_{y,y} + \delta_{x,x'-1}\delta_{y,y'}\right] \\ &- \mu\left[\delta_{x,x'}\delta_{y,y'}\right], \end{aligned} \tag{38}$$

Similar to the one-dimensional chain, we can perform a Fourier transformation and as a result from applying this and the Kronecker δ relation:

$$H_{k_x,k_y} = -2t\left(\cos\left(k_x\alpha\right) + \cos\left(k_y\alpha\right)\right) - \mu. \tag{39}$$

As with the chain in 3.1 we can then conclude that the eigenenergies are given by:

$$E_k = -2t\left(\cos\left(k_x\alpha\right) + \cos\left(k_y\alpha\right)\right) - \mu. \tag{40}$$

3.2.1 Approximating the Eigenenergies

From Eq. (40) we can try to take the approximate expression for low momenta which requires a chemical potential $\mu \approx -4$. As found in Eq. (24) we can approximate the eigenenergies for the square lattice:

$$E_k \approx -t\alpha^2 \left(k_x^2 + k_y^2\right) - \bar{\mu}, \tag{41}$$

where we again set $\bar{\mu} = 0$ similar to the one-dimensional situation.

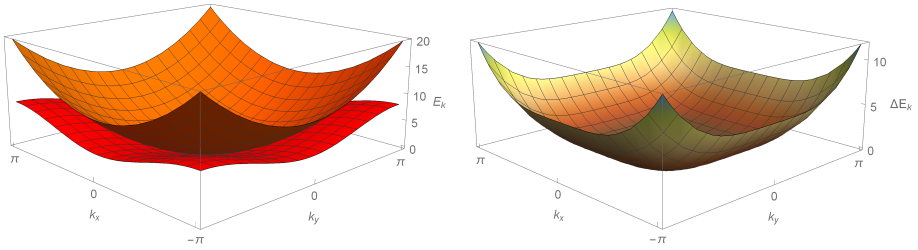

(a) (b)

Figure 6: **(a)**: The exact and approximate eigenenergies shown in red and orange respectively. Here $\mu = -4$ for the exact eigenenergy.
(b): The difference between the two functions as a colorfunction.

As can be seen the functions are very similar for low momenta. It is useful however to check when the approximation is no longer expected to give a representative result. From the quadratic dispersion we know it will always have a circular Fermi surface, no matter at what energy the system is. The exact result is only circular for low momenta. In Fig. 7 we can see that the Fermi surface is circular to good approximation for $\mu \approx -4$. At $\mu \approx -2$ we can see some morphing and the surface becomes more square-like. At $\mu = 0$ the surface has become perfectly square and we expect the results coming from the exact and approximation to be entirely different.

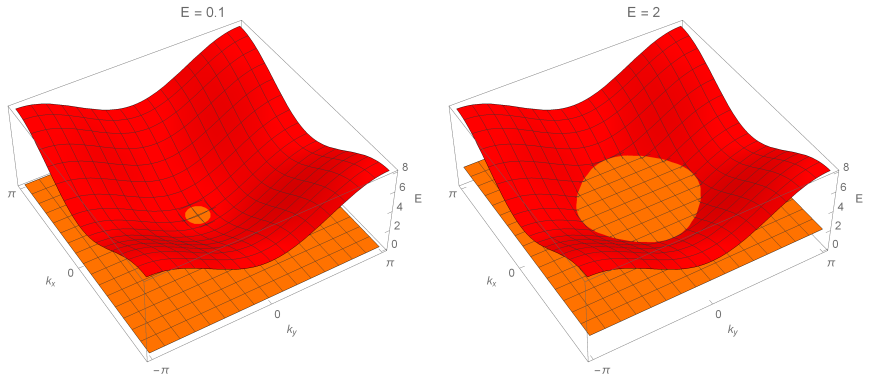

(a) (b)

(c)

Figure 7: The Fermi surface for low, intermediate and high energies.

3.2.2 The Density of States

Similar to the one-dimensional case we will start with our approximation for the eigenenergies

$$E_k = t\alpha^2 \left(k_x^2 + k_y^2\right).$$

Using this in combination with our expression for the Green's function and LDOS from Eqs. (16) and (20) we can start out with

$$G_0^R\left(x, y, E\right) = \lim_{\eta \to 0^+} \iint \frac{d\vec{k}}{\left(2\pi\right)^2} \frac{e^{i\vec{k}\cdot\vec{r}}}{\omega - t\alpha^2\vec{k}^2},$$

where $\vec{k} = (k_x, k_y)$ and $\vec{r} = (x, y)$ and remind ourselves that $\omega = E + \mu$. From this point on our approach will be different as we cannot use the Residue theorem. Switching to cylindrical coordinates results in

$$G_0^R(r, \theta, E) = \lim_{\eta \to 0^+} \int_0^{2\pi} \int_0^{\infty} \frac{d\kappa d\theta}{(2\pi)^2} \frac{\kappa \exp\left[i\kappa r \left(\sin(\theta)\sin(\phi) + \cos(\theta)\cos(\phi)\right)\right]}{\omega - t\alpha^2\kappa^2},$$

in which we have used $k_x = \kappa\cos(\theta)$ and $x = r\cos(\phi)$ and similar substitutions for k_y and y. Using the product-to-sum identities for $\sin(\beta)$ and $\cos(\beta)$ we get $e^{i\vec{k}\cdot\vec{r}} = e^{i\kappa r\cos(\theta-\phi)}$ and combining this with the fact that we are integrating θ over 2π we can discard ϕ and shift θ to $\theta + \frac{\pi}{2}$ which converts $\cos(\theta)$ to $-\sin(\theta)$;

$$G_0^R(r, \theta, E) = \lim_{\eta \to 0^+} \int_0^{2\pi} \int_0^{\infty} \frac{d\kappa d\theta}{(2\pi)^2} \frac{\kappa \exp\left[-i\kappa r \sin(\theta)\right]}{\omega - t\alpha^2\kappa^2}.$$

The θ-integral can be recognized as a Bessel function $J_0(x)$ and then the κ-integral results in the $K_0(x)$ Bessel function and this gives us the final result:

$$\begin{aligned} G_0^R(r, E) &= \lim_{\eta \to 0^+} \int_0^{\infty} \frac{d\kappa}{2\pi} \frac{\kappa J_0(\kappa r)}{\omega - t\alpha^2\kappa^2} \\ &= \lim_{\eta \to 0^+} -\frac{1}{2\pi t\alpha^2} K_0\left(r\sqrt{-\frac{\omega}{t\alpha^2}}\right). \end{aligned} \tag{42}$$

The real part of the $K_0(x)$ Bessel function tends to infinity for small r. Luckily, this is not an actual problem, as the imaginary part is relevant and it remains finite. For $r \to 0$ we see that $K_0\left(r\sqrt{-\frac{\omega}{t\alpha^2}}\right) \to \frac{\pi}{2}$. To verify we can calculate the bare density of states in a different way:
Let us start with

$$\begin{aligned} \rho_0(E) &= -\frac{1}{\pi}\mathrm{Im}\left[\iint \frac{d^2k}{(2\pi)^2} \frac{1}{\omega - t\alpha^2k^2}\right] \\ &= -\frac{1}{\pi}\mathrm{Im}\left[\int_0^{\infty} \frac{dk}{2\pi} \frac{k}{\omega - t\alpha^2k^2}\right] \\ &= -\frac{1}{\pi t\alpha^2}\mathrm{Im}\left[\int_0^{\infty} \frac{d\kappa}{2\pi} \frac{\kappa}{\omega - \kappa^2}\right]. \end{aligned}$$

Now we use that $\lim_{\eta \to 0^+} \frac{1}{E + i\eta + \mu - E_k} = -i\pi\delta(E + \mu - E_k)$ and have rescaled $\kappa^2 = t\alpha^2k^2$.

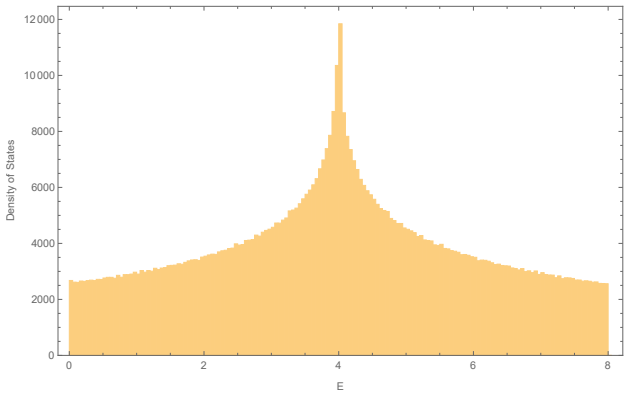

Figure 8: A histogram of the density of states for a dk_x and dk_y of $\frac{\pi}{400}$.

$$\begin{aligned}\rho_0(E) &= \frac{1}{\pi t\alpha^2}\mathrm{Re}\left[\int_0^\infty d\kappa\,\kappa\,\delta\left(E+\mu-\kappa^2\right)\right] \\ &= \frac{1}{2\pi t\alpha^2}\mathrm{Re}\left[\int_0^\infty d\kappa\,\kappa\frac{\delta(\kappa_0-\kappa)}{|2\kappa|}\right] \\ &= \frac{1}{4\pi t\alpha^2}.\end{aligned} \tag{43}$$

This indicates the density of states is a constant and reassures us of the correctness of the Green's function in Eq. (42).

3.2.3 Comparison of the Exact and Approximate Density of States

To compare the approximate result with the exact we will turn to numerical results from a model in **Mathematica**. Here we have set up a 100×100 lattice. We set up a matrix for the Hamiltonian analogous to Eq. (39) with small discrete steps for dk_x and dk_y from $-\pi$ to π. From there on out we use a route similar to the one discussed in Section 2.3. As found in the previous section, the density of states is a constant both with respect to space and the eigenenergies for low chemical potential. Numerically we find that this true in that regime as well. In Fig. 8 we can see that for low energies the density of states can be approximated as flat.

4 A Monatomic Chain with an Impurity

In this section we will include an impurity in the monatomic chain and look at how this changes the characteristics of the density of states. Both a repulsive and attractive potential will be discussed in that order. We will calculate the approximate density of states analytically and then turn to numerics for the exact density of states. At the end we will conclude with a comparison of the results.

4.1 The Local Density of States

4.1.1 The Approximate Local Density of States

Now that we have found an expression for the bare Green's function $G_0^R(x,E)$, we can find the function for the DOS due to an impurity (IDOS) $\rho_I(\vec{r},E)$;

$$\rho_I(\vec{r},E) \equiv -\frac{1}{\pi}\lim_{\eta\to 0^+}\mathrm{Im}\left[G_0^R(\vec{r},E)\,T(E)\,G_0^R(\vec{r},E)\right]. \tag{44}$$

Let us take a monatomic chain with an impurity at one site (Fig. 9) separated by a lattice constant α. Suppose we have an impurity at $x=0$[7]. In continuous

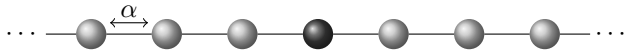

Figure 9: A monatomic chain with an impurity at one site.

space we can describe such an impurity with a Dirac delta function:

$$H_I = V_0\delta(x).$$

This allows us to concretely set up our T-matrix according to Eq. (13)

$$T(E) = \left(1 - G_0^R(0,E)\,V_0\right)^{-1}V_0. \tag{45}$$

This matrix is only non-zero for $x=0$. As such, we can treat it as a number instead of a matrix. Using the bare Green's function found in Section 3.1.2 we find for the IDOS:

$$\begin{aligned}\rho_I(x,E) &= -\frac{1}{\pi}\lim_{\eta\to 0^+}\mathrm{Im}\left[G_0^R(x,E)\,T(E)\,G_0^R(-x,E)\right]\\ &= -\frac{1}{\pi}\lim_{\eta\to 0^+}\mathrm{Im}\left[-\frac{1}{4t\alpha^2\omega}\exp\left(2i\sqrt{\frac{\omega}{t\alpha^2}}|x|\right)T(E)\right],\end{aligned} \tag{46}$$

[7] This may be a different atom or a vacancy at the position $x=0$

where $T(E) = \left(1 - G_0^R(0,E)\, V_0\right)^{-1} V_0$. With the bare density of states $\rho_0(E)$ from Eq. (33) and the IDOS $\rho_I(x,E)$, we can assemble the LDOS:

$$\begin{aligned}\rho(x,E) &= \rho_0(E) + \rho_I(x,E) \\ &= \frac{1}{2\pi}\left(\mathrm{Im}\left[i\sqrt{\frac{1}{t\alpha^2\omega}} + \frac{1}{2t\alpha^2\omega}\exp\left(2i\sqrt{\frac{\omega}{t\alpha^2}}|x|\right)T(E)\right]\right) \end{aligned} \tag{47}$$

4.1.2 Low Energies

The graphs below are all evaluated with $\mu = -2$. Here η has been set to 0.08. The size of η is very much related to the system size as it will destabilize the numerical model. Due to this we cannot choose η extremely small. For low energies we would expect the expression in Eq. (46) to match with the exact result. In Fig. 10 we can see the results match up very well. Note that for negative energies there is no oscillation in the IDOS as the particle does not have the energy to occupy closeby states.

4.1.3 Higher Energies

For higher energies we saw in Section 3.1.1 that there is a clear difference between the eigenenergies. In Fig. 11 we can see that this already starts to form at $\mu = -1.5$. For $\mu = -1.0$ this becomes more evident and for $\mu = 0$ the starting amplitude is nearly halved.

4.1.4 An Attractive Potential

An attractive potential is a different . For such a potential it is important that V_0 is not too negative or it will cancel itself out as can be seen in Eq. (45) which would reduce to ${}^{-1}/_{G_0^R(0,E)}$. For this situation we will choose a slightly attractive potential V_0 (Fig. 12). The graphs show the results again agree for low energies but the discrepancy comes up for higher energies.

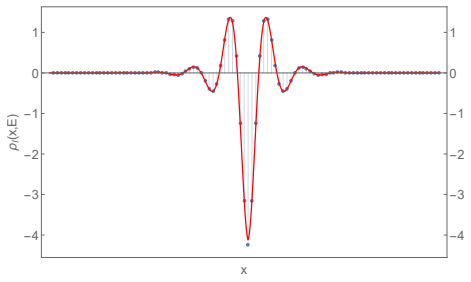

Figure 10: The IDOS for a repulsive potential for $\mu = -3.9$.

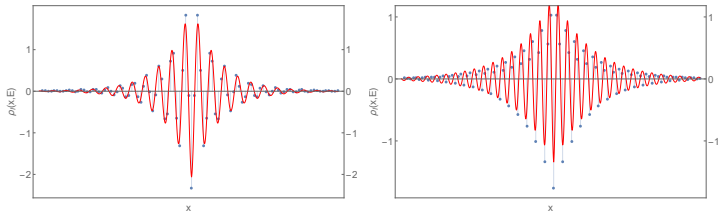

(a) (b)

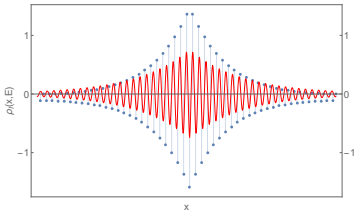

(c)

Figure 11: The IDOS for a repulsive potential.
(a): $\mu = -1.5$. **(b)**: $\mu = -1.0$. **(c)**: $\mu = 0$.

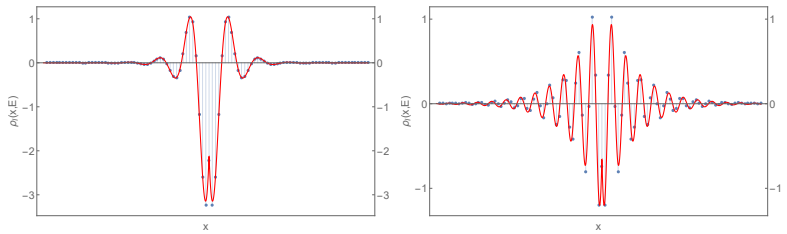

(a) (b)

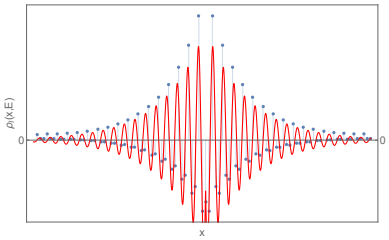

(c)

Figure 12: The IDOS for an attractive potential.
(a): $\mu = -1.9$. **(b)**: $\mu = -1.5$. **(c)**: $\mu = -1.0$.

5 A Square Lattice with an Impurity

This section is analogous to the previous, but will treat the case of a square lattice with solely a repulsive potential. We will find the approximate LDOS analytically with the quadratic dispersion found in Section 3.2.1 and then find the numerical results for the exact density of states. Unlike the monatomic chain we will also look at the density of states in momentum space. We will conclude with a comparison of the results.

5.1 The Local Density of States

5.1.1 The Approximate Local Density of States

Similar to earlier we will insert an impurity at one site in the lattice (see Fig. 13).

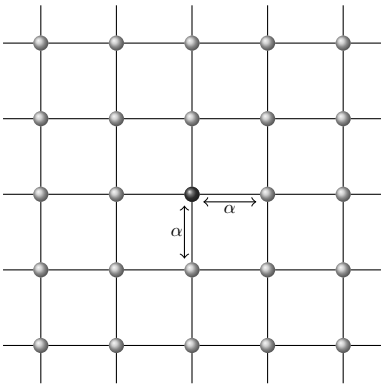

Figure 13: A square lattice with an impurity at one site.

Now using Eq. (42) we find for the IDOS:

$$\rho_I(r,E) = -\frac{1}{\pi}\mathrm{Im}\left[\left(\frac{1}{2\pi t\alpha^2}\right)^2 K_0^2\left(r\sqrt{-\frac{\omega}{t\alpha^2}}\right)T(E)\right], \tag{48}$$

where $T(E) = (\mathbb{I} - G_0^R(E)H_I)^{-1}H_I$ and $H_I = V_0\delta(x,y)$. Complementing this with the bare density of states from Eq. (43), we can find the LDOS:

$$\begin{aligned}\rho(\vec{r},E) &= \rho_0(E) + \rho(\vec{r},E)\\ &= \frac{1}{4\pi t\alpha^2} - \frac{1}{\pi}\mathrm{Im}\left[\left(\frac{1}{2\pi t\alpha^2}\right)^2 K_0^2\left(r\sqrt{-\frac{\omega}{t\alpha^2}}\right)T(E)\right].\end{aligned}$$

5.1.2 Low Energies

For a 100×100 lattice the LDOS with an impurity inserted at the center of the lattice is known. In Fig. 14 both IDOSs can be seen. While the exact IDOS clearly has stronger oscillations of a shorter wavelength than the approximate IDOS. This is not unexpected as our approximation was for low energies, i.e. low k. This means it will work well for longer wavelengths in real space and as $r \to \infty$ we see that the results do match up.

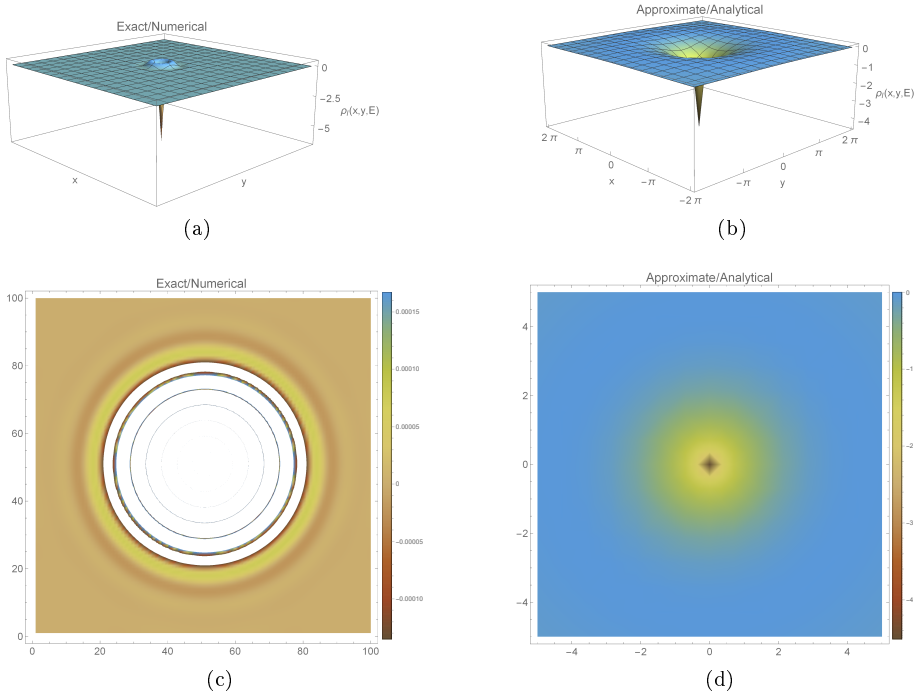

Figure 14: Plots for the exact and approximate IDOS for $\mu = -3.9$
(a): Plot of the numerical result for the exact IDOS.
(b): Plot of the analytical result for the approximate IDOS.
(c): Density plot of the numerical result for the exact IDOS.
(d): Density plot of the analytical result for the approximate IDOS.

5.1.3 Higher Energies

For higher energies however, there is a clear difference (Fig. 15) . The exact solution now clearly lacks rotational symmetry and it is easy to see the IDOS does not depend on r but on x and y separately.. This is due to the fact that the model is a square lattice and not an actual rotationally symmetric crystal. The approximation does assume such symmetry (it depends on r instead of x and y separately) which explains its shape even at higher energies and is no longer a reliable alternative.

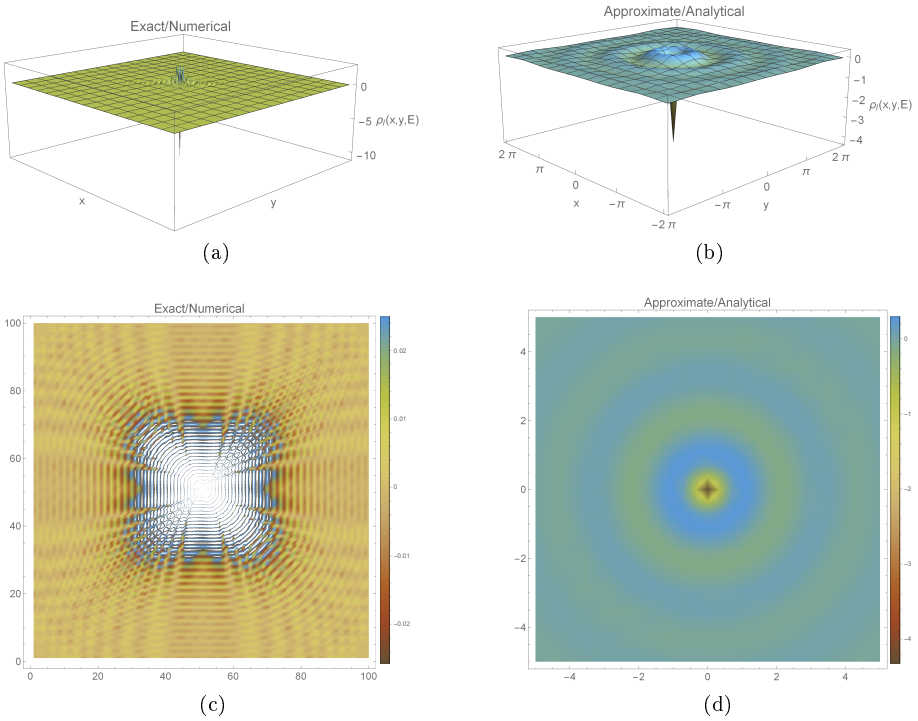

Figure 15: Plots for the exact and approximate IDOS for$\mu = -2$:
(a): The numerical IDOS.
(b): The analytical IDOS.
(c): Density plot of the numerical IDOS.
(d): Density plot of the analytical IDOS.

This pattern continues as we look at $\mu = 0$ (Fig. 16). We can now see in the exact IDOS that there is a profound aversion to sit at positions where $x = y$.

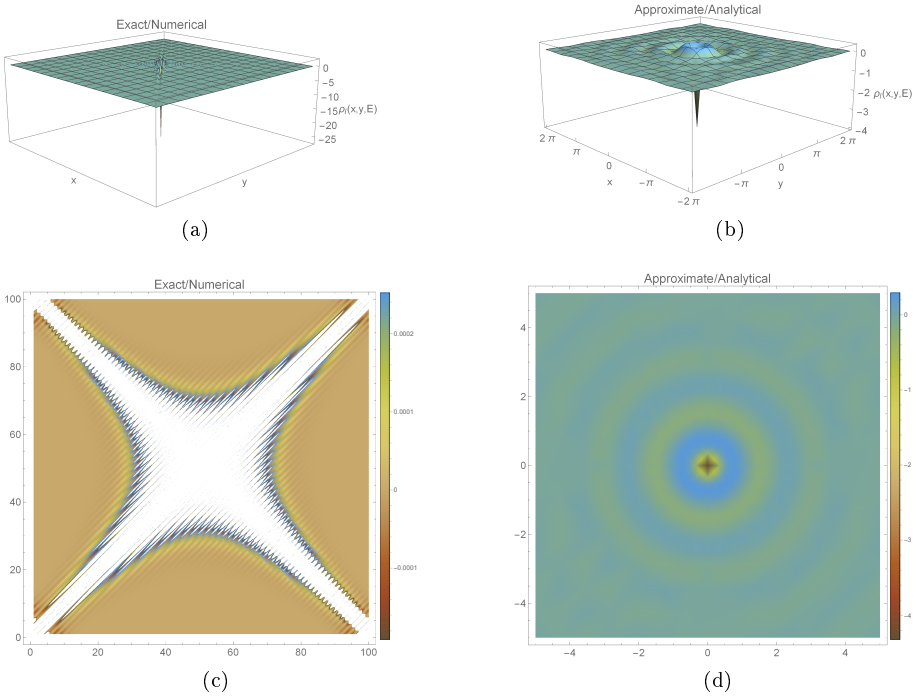

(a) (b)

(c) (d)

Figure 16: Plots for the exact and approximate IDOS for $\mu = 0$:
(a): Plot of the numerical result for the exact IDOS.
(b): Plot of the analytical result for the approximate IDOS.
(c): Density plot of the numerical, exact IDOS.
(d): Density plot of the analytical, approximate IDOS.

5.2 The Fourier-Transformed Local Density of States

An interesting quantity is the Fourier-transformed local density of states (FT-LDOS). It shows the probability to scatter at certain momenta $\vec{k}$ which relies on the energy of the incoming particle. To this end we will Fourier-transform the density of states due to the impurity (FT-IDOS) and then compare it to the numerical result.

5.2.1 The Approximate Fourier-Transformed Local Density of States

The FT-IDOS is given by:

$$\rho_I\left(\vec{k},E\right) = -\frac{1}{\pi}\mathrm{Im}\left[\iint \frac{d\vec{r}}{(2\pi)^2}\rho_I\left(r,E\right)e^{i\vec{k}\cdot\vec{r}}\right].$$

Similar to the derivation in Section 3.2.2 we can rewrite the exponent $e^{-i\vec{k}\cdot\vec{r}} = e^{-ikr\cos(\theta)}$;

$$\begin{aligned}
\rho_I\left(k,\theta,E\right) &= -\frac{1}{\pi}\mathrm{Im}\left[\iint \frac{d\theta dr\, r}{\left(2\pi t\alpha^2\right)^2}K_0^2\left(r\sqrt{-\frac{\omega}{t\alpha^2}}\right)T\left(E\right)e^{-ikr\cos(\theta)}\right] \\
&= -\frac{1}{\pi}\mathrm{Im}\left[\int_0^\infty \frac{dr\, r}{2\pi\left(t\alpha^2\right)^2}J_0\left(kr\right)K_0^2\left(r\sqrt{-\frac{\omega}{t\alpha^2}}\right)T\left(E\right)\right] \\
&= -\mathrm{Im}\left[\frac{T\left(E\right)}{\pi^2\left(t\alpha^2\right)^{3/2}k\sqrt{4\omega - t\alpha^2k^2}}\mathrm{arcsinh}\left(\sqrt{\frac{t\alpha^2}{\omega}}\frac{k}{2}\right)\right]. \qquad (49)
\end{aligned}$$

5.2.2 Low Energies

Now that there is an expression for the FT-IDOS it can be compared to the exact result. As can be seen in Fig. 17 similar to the IDOS the FT-IDOS approximation and exact solution agree for low energies ($\mu = -3.9$). Both show a steep, circular peak around the origin.

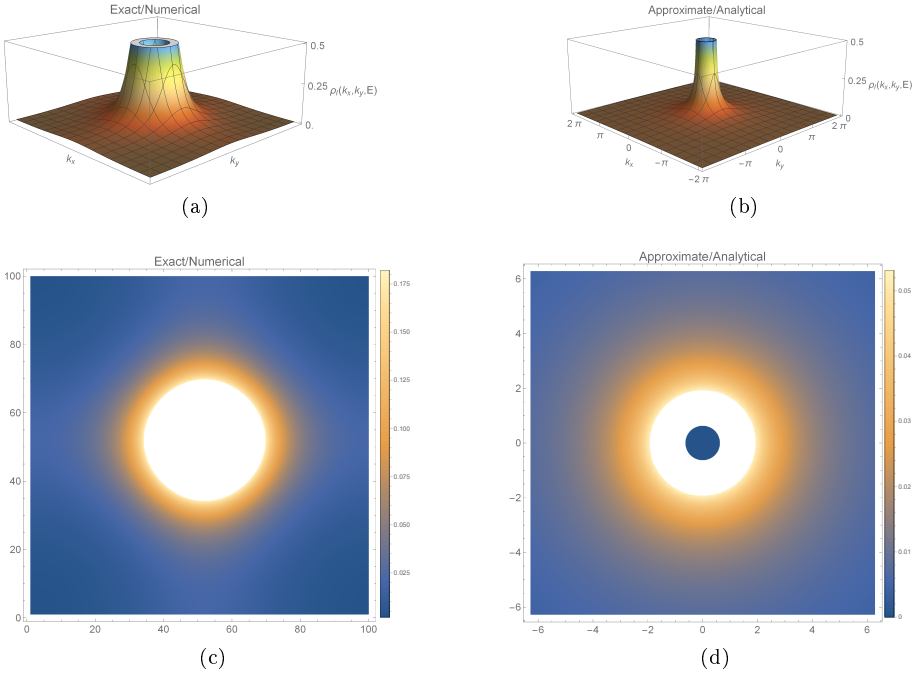

Figure 17: Plots for the exact and approximate FT-IDOS for $\mu = -3.9$:
(a): Plot of the numerical result for the exact FT-IDOS.
(b): Plot of the analytical result for the approximate FT-IDOS.
(c): Density plot of the numerical FT-IDOS.
(d): Density plot of the analytical FT-IDOS.

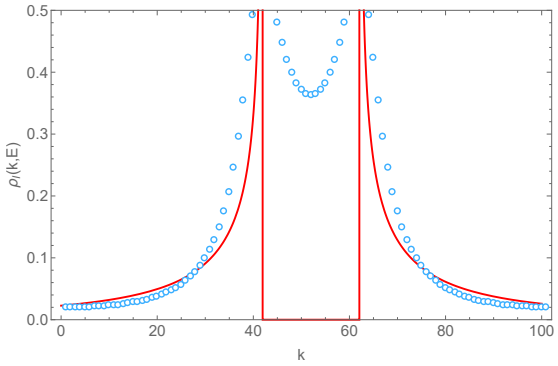

Figure 18: Overlay plot showing the numerical data in blue and analytical result in red. The width of the peaks match up very well. This peak is located at the scattering momentum.

Comparing the graphs in Fig.17 can be tricky, but remarkably for this energy the approximation seems to represent reality better as the density plot shows the center is actually zero. The numerics have trouble with the peak so close to the origin and the centet is not actually equal to zero. In Fig. 18 a cross-section of both FT-IDOSs show that their peaks do line up very well. The radius of the circle is related to the energy. This can be seen from Eq. (49) where the density of states shoots off to infinity for $4\omega - t\alpha^2 k^2 = 0$. For the analytical result we can see that the peak should be located at $k^2 = \frac{4\omega}{t\alpha^2}$. For $\omega = 0.1$ and $\alpha = t = 1$ this corresponds to $k^2 = 0.4$ or $k \approx 0.632$. The radius of the circular peak is 10 discrete steps of $\frac{2\pi}{N}$. For $N = 100$ this corresponds to $k = 10 \cdot \frac{2\pi}{100} \approx 0.628$. This explicitly shows how well the two methods agree for low momenta.

5.2.3 Higher Energies

For higher energies the exact solution shows a very different pattern. This is due to the square nature of the model. The approximation does not account for this and keeps its rotational symmetry (Fig. 19). The discrepancy becomes more clear in Fig. 20 where we can see that there is a difference between the peaks. The analytical peak is situated at $k = \sqrt{8} \approx 2.82$. The peak for the numerical result is 50 discrete steps from the origin, which means $k = 50 \cdot \frac{2\pi}{100} \approx 3.14$. As expected we already see a significant difference. It is safe to say that for $\mu \leq 2$ the quadratic dispersion is no longer as reliable.

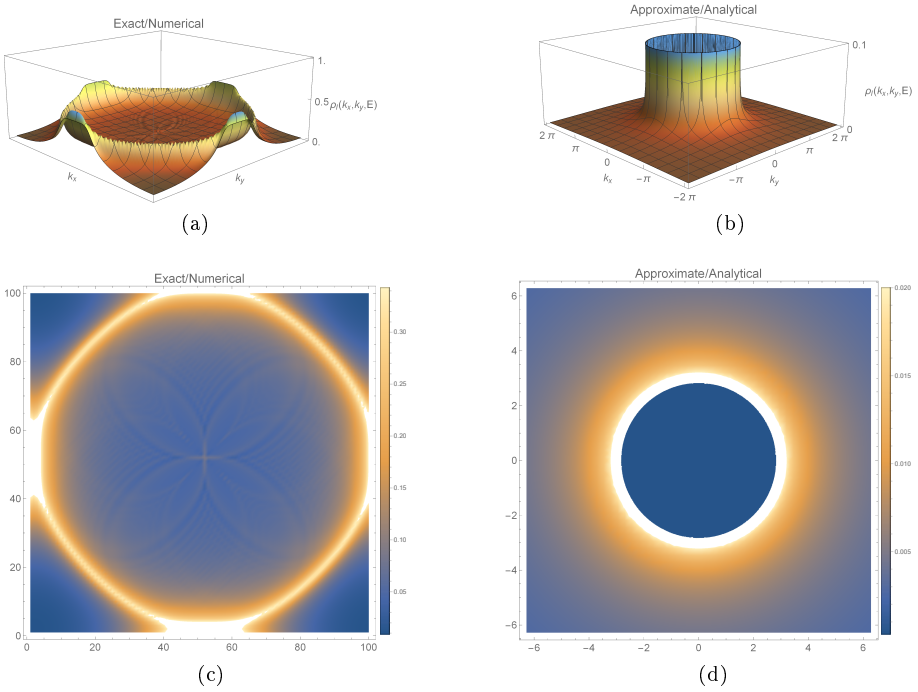

(a) (b) (c) (d)

Figure 19: Plots for the exact and approximate FT-IDOS for $\mu = -2$:
(a): The numerical FT-IDOS.
(b): The approximate FT-IDOS. The chopped look of the approximate result is due to **Mathematica** having trouble with the divergence at $4\omega - t\alpha^2 k^2 = 0$.
(c): A density plot of the numerical FT-IDOS.
(d): A density plot of the analytical FT-IDOS.

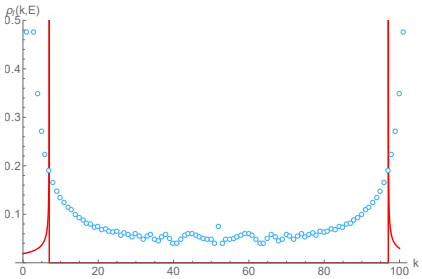

Figure 20: Overlay plot showing the numerical data in blue and analytical result in red. The scattering momenta do not match up as well as for $\mu = -3.9$.

To look at the extreme case we can also evaluate $\mu = 0$. As can be seen in Figure 21. the analytical solution continues to expand the radius of the peak.

The numerical solution however shows a completely different behavior. It is high where $k_x^2 = k_y^2$ and low where this significantly differs. This is due to the Fermi surface that is now a square and can no longer be represented with a quadratic dispersion.

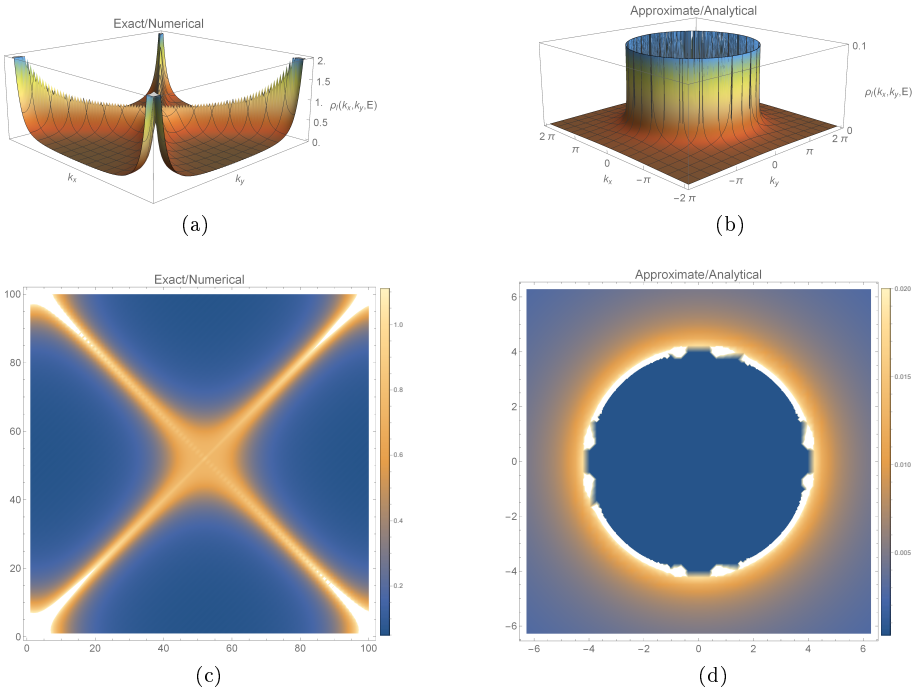

(a) (b)

(c) (d)

Figure 21: Plots for the exact and approximate FT-IDOS for $\mu = 0$:
(a): Plot of the numerical result for the exact FT-IDOS.
(b): Plot of the analytical result for the approximate FT-IDOS.
(c): Density plot of the numerical, exact FT-IDOS.
(d): Density plot of the analytical, approximate FT-IDOS.

6 Conclusion

This section will conclude the thesis by evaluating the results found in Sections 4 and 5. Specifically the reliability of the approximation for low energies will be discussed and when it is still legitimate to make use of the approximation. An outlook for future research will then be given as a final thought.

6.1 Results

The thesis was aimed towards finding the effects of an impurity in a crystal. In the first section it familiarizes us with the Green's function and shows its use by relating it to the density of states. The next section neatly follows up on this by finding the eigenenergies required to perform the calculations. As the exact solution cannot always be calculated analytically it grants a useful alternative to finally find the density of states for a regular monatomic chain and square lattice. The final and most significant results are found in the last two sections where the impurities are implemented. It is safe to conclude that an impurity radically alters the behavior of the crystal in close proximity to the impurity. Most importantly the density of states implies preferred positions and momenta when scattering occurs. The approximation made has allowed us to get analytical results which are reliable for $\mu > -2$, but fail for higher chemical potentials.

6.2 Outlook

More research could be conducted by looking at three-dimensional systems and making a distinction between the surface and bulk of such crystals. Among other things spin, more impurities, bound states and more complex potentials could also be a point of interested that has physical significance. The problem of numerics is still there and the choppy density plots are a direct result. Increasing the amount of plot points and maximum recursion combat this quite well, but significantly increase the calculation time so more powerful computing could be an answer. A second issue is that the exact solution cannot be calculated analytically. This limits the research to either low energies or numerics.

Layman's Summary

Most solids have a certain geometry on a microscopic scale. This geometry combined with the actual atoms determine many properties of these solids. A common known implementation of this are alloys where two (or more) metals are combined to create an often stronger material[2]. The thesis aims at calculating how an impurity (i.e. a different atom or no atom at all) in one place of this geometric structure affects the density of states. The density of states gives a lot of information about a material. It can for example make the distinction between conductors, semiconductors and insulators. The density of states $\rho(x, E)$ can be interpreted as a probability for a particle to be at position x when it has energy E.

Section 2 is the most mathematical. It introduces the Green's function and shows how it can be used to find the density of states. The Green's function is a function that solves a specific kind of equation. The Schroedinger equation falls among this kind and makes it such a powerful tool for us.

In Section 3 we start looking at the lattices. We first look at an infinitely long chain of atoms at the same distance from each other. We want to find the density of states for the pure crystals. To do so we first calculate the energies that the system can hold and make an approximation that we will need to continue analytically (instead of numerically). The energies are called eigenenergies and are needed for the expression found in the previous section for the density of states, we then repeat this for an infinitely long lattice of atoms again at the same distance apart.

In Section 4 and 5 we treat the one-dimensional and two-dimensional case where there is an impurity separately. The impurities make the system spatially dependent and we expect the density of states to be varying as we move away or towards the impurity. In the second part of the square lattice section we also look at the density of states $\rho(k, E)$ as a function of the momentum k instead of the position x. This should then be interpreted as the probability for a particle to be scattered away at a momentum k when it has energy E.

References

[1] The Nobel Prize Organization, *The Nobel Prize in Physics 2010*, https://www.nobelprize.org/nobel_prizes/physics/laureates/2010/

[2] Callister, W.D., *Materials Science and Engineering: An Introduction*, John Wiley and Sons, Inc New York, 2007.
ISBN: 978-1-118-31922-2

[3] Altland, A. and Simons, B.D., *Condensed Matter Field Theory*, Cambridge University Press, 2006.
ISBN: 978-0-511-78928-1

[4] van Dalum, G.A.R., *Phase transitions of the Swedenborgite antiferromagnet & quasiparticle interference in a topological insulator,* Master's thesis, Utrecht University, 2016.

[5] Economou, E.N., *Green's Functions in Quantum Physics*, Springer, 2006.
ISBN: 978-3-540-28841-1

[6] Whitaker, E.T. and Watson, G.N., *A Course of Modern Analysis*, Cambridge University Press, 1962.
ISBN: 978-0-521-09189-3

[7] Ashcroft N.W. and Mermin, N., *Solid State Physics*, Cengage Learning, Inc, 1976.
ISBN: 978-0-030-83993-1

[8] Griffiths, D.J., *Introduction to Quantum Mechanics*, Cambridge University Press, 2013
ISBN: 978-1-292-02408-0